

Robust Control of Cart-Pendulum Dynamics against Uncertain Multiple Time Delays

Mursel Emre Cavdaroglu, *Member, ASME-IEEE*, Nejat Olgac, *Fellow, ASME, Senior Member, IEEE*

¹*Abstract*— We consider a fixed control law on a well-known underactuated dynamics, the cart-and-pendulum system. The contributory aspect of this research which is different from the traditional treatment is that, the feedback line is affected by multiple independent time delays. It is known that time-delayed LTI systems may exhibit multiple stable operating zones (pockets) in the space of delays. But finding these pockets analytically and demonstrating them experimentally are complex and challenging problems. The main aim of this effort is to accomplish a successful trajectory tracking on a practical, underactuated mechanical system under the presence of multiple time delays. First, we model the system as precisely as we can and over this model we use a powerful methodology for handling the delays. This method is called *cluster treatment of characteristic roots (CTCR)* which reveals the stability pockets in the delay space. Then, we experimentally verify the analytical findings of CTCR. As a novel contribution to the controls area, this study shows that underactuated systems with multiple delays may exhibit better performance (such as faster disturbance rejection capability) for larger delay values when they are properly selected. This is a counter-intuitive outcome of the study, and it enables us to utilize ‘*delay scheduling*’ procedure. In delay scheduling, we declare the set of larger delays (than those that are present) for which the control routine performs better. This procedure offers to the control system designer a powerful tool.

Nomenclature

x	Cart position (m)	n	Gear box ratio
θ	Pendulum angle from the upright position (rad)	R	Motor armature resistance (Ω)
x_d	Desired trajectory for x (m)	r	Driver pinion radius (m)
θ_d	Desired trajectory for the pendulum angle (rad)	M	Mass of the cart (kg)

¹This research has been supported in part by the awards from DoE (DE-FG02-04ER25656), NSF (CMS-0439980) and NSF (DMI-0522910).

Mursel E. Cavdaroglu is with the Mechanical Engineering Department, University of Connecticut, Storrs, CT 06269-3139, USA (e-mail: emre@engr.uconn.edu).

Nejat Olgac is with the Mechanical Engineering Department, University of Connecticut, Storrs, CT 06269-3139, USA (Phone: (860) 486 2382, e-mail: olgac@engr.uconn.edu).

V_m	Voltage applied to the DC motor of the cart (V)	I	Pendulum moment of inertia about its center of gravity (kgm^2)
F	Force applied to the cart (N)	m	Mass of the pendulum (kg)
b	Equivalent viscous friction constant for the cart (Ns/m)	l	Half length of the pendulum (m)
b_0	Equivalent coulomb friction force on the cart (N)	g	Gravitational acceleration (m/s^2)
F_{fric}	Nonlinear frictional force on the cart (N)	c	Viscous friction constant for the pendulum hub (Nms/rad)
K_e	Motor back-emf constant (Vs)	c_0	Coulomb frictional torque on the pendulum hub (Nm)
K_t	Motor torque constant (Nm/A)	T_{fric}	Nonlinear frictional torque on the pendulum hub (Nm)

I. INTRODUCTION

Stabilization of underactuated cart-pendulum systems has been an important and popular problem in controls area for several decades [1, 2, 7, 8, 15, 17]. In this paper, we deal with the problem from a novel perspective. The novelty is in the introduction of multiple feedback delays within the controlled dynamics and the ‘scheduling’ of these delays for improved system performance. The main objective is to analyze and verify the effect of time delays on the tracking performance of the cart-and-pendulum dynamics. We claim a smart ‘delay scheduling’ methodology, which proposes adding appropriate amounts of artificial delays to the feedback line in order to improve the performance.

Underactuated systems are the control systems with fewer actuators than the number of degrees-of-freedom. Examples of this kind of systems can be found in many applications such as biology, flexible-link robots, mobile robots, cars, aircrafts, helicopters, satellites, and underwater vehicles. As a specific and popular example, the cart-and-pendulum system is a simple underactuated robotic structure with a two degree-of-freedom dynamics as shown in Fig. 1. The cart has a control force that is applied by a DC servo motor, while the pendulum reacts to the motion of the cart. The motor is driven within a high-speed digital control loop using a PD controller. The pendulum is made of a simple slender rod and it is mounted on the cart. The position of the cart is monitored by an optical encoder (Encoder A in Fig. 1) attached to the geared wheel of the cart. The angular position of the pendulum is also measured via another optical encoder (Encoder B in Fig. 1). The velocities of the cart and the pendulum are calculated numerically from these encoder signals utilizing a noise reduction filter.

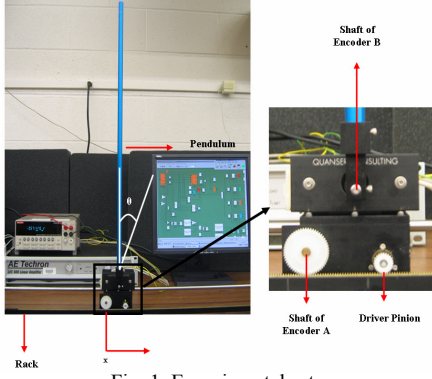


Fig. 1. Experimental setup.

Most of the control treatments for the cart-and-pendulum system include geometric nonlinear control, as well as methods based on passivity and energy for stabilization and swinging up the pendulum [1, 2, 15]. Also fixed point backstepping method is used on the stabilization of inverted pendulum as an example to the special class of cascaded underactuated nonlinear systems [8]. In this paper, we deal with the trajectory tracking control for the cart while maintaining the pendulum in the upright position ($\theta = 0$) using a full state feedback law. The operation is considered successful if the position of the cart follows a defined trajectory while keeping the angle of the pendulum as close to zero as possible. The treatment here starts from the initial equilibrium configuration with the pendulum is in the upright position. The fixed control law to achieve this is designed based on the non-delayed linear system using the LQR optimum control design methodology. We perform a componentwise system identification effort on the setup and obtain a relatively accurate model. This model also gives a reasonable simulation environment for comparison studies against the experimental results.

As the crucial novelty in this study, we consider the feedback information with multiple time delays. Some earlier studies on this problem include single time delay in the feedback line [3, 5, 7]. The effects of a PD controller and a delayed P controller on the stability performance are compared in [3]. And in [7], the critical delay value which leads to the marginal stability condition is found experimentally. In another study, the destabilizing effect of time delay (which is treated as a communication delay) is compensated by using state estimators [5]. It's a very challenging problem to determine the stability disposition of the delayed control of the cart-and-pendulum system when there are multiple delays, which are fixed but uncertain. We follow a recent methodology of our group, which is called the *cluster treatment of characteristic roots (CTCR)* [10, 13, 14]. We briefly explain the key propositions of CTCR. Then, we verify the analytically obtained stability map on the cart-and-pendulum experimental setup. An interesting outcome of this work appears as, we observe that the dynamics may exhibit better performance with larger time delays for a fixed control logic. The contributory points of this paper are the stability robustness declaration in the domain of uncertain multiple delays, determination of the optimum delay values for the best tracking performance and

the 'scheduling of the delays'.

The outline of the paper is as follows: In Part 2, the full mathematical model and the componentwise identification of the cart-and-pendulum system are described. Then, the controller for the non-delayed feedback structure is designed and effect of the delays on the stability is analyzed by utilizing CTCR in Part 3. In Part 4, the claims of this paper are verified experimentally on the setup with trajectory tracking and disturbance rejection tests.

I. DYNAMIC MODEL AND COMPONENTWISE SYSTEM IDENTIFICATION

The nonlinear mathematical model of the cart-and-pendulum system is adapted from [6] as:

$$F = (M + m)\ddot{x} + m\ell\ddot{\theta}\cos\theta - m\ell\dot{\theta}^2\sin\theta + F_{fric} \quad (1)$$

$$(I + m\ell^2)\ddot{\theta} + T_{fric} + m\ell\ddot{x}\cos\theta = mg\ell\sin\theta \quad (2)$$

where $I = \frac{m\ell^2}{3}$ and all the terms are described in the nomenclature. Considering small angular excursions for the pendulum, equations (1) and (2) are linearized as:

$$F = (M + m)\ddot{x} + m\ell\ddot{\theta} + F_{fric} \quad (3)$$

$$(I + m\ell^2)\ddot{\theta} + T_{fric} + m\ell\ddot{x} = mg\ell\theta \quad (4)$$

The feedback control force, F , stabilizes the pendulum at the upright configuration ($\theta = 0$), which is an unstable equilibrium for the uncontrolled system [8]. The force (F) which is generated by the motor on the cart, is modeled considering the back-emf and the armature voltage (V_{in}) as:

$$F = \frac{V_{in}K_t n}{Rr} - \frac{K_t K_e n^2 \dot{x}}{Rr^2} = \alpha V_{in} - \beta \dot{x} \quad (5)$$

where α and β are self evident constants.

A. Componentwise System Identification

Motor parameters, nonlinear friction characteristics of the rack-pinion drive and the pendulum hub friction are carefully studied for a good representation of the system and a meaningful simulation effort. We review this study next.

Friction between the rack and pinion is modeled as a combination of viscous and coulomb frictions as follows:

$$F_{fric} = b\dot{x} + F_c \quad (6)$$

where F_c is the nonlinear dry friction force and it is defined as:

$$F_c = \begin{cases} b_0 \operatorname{sgn}(\dot{x}), & \dot{x} \neq 0, \text{ Coulomb friction} \\ F, & \dot{x} = 0, \text{ Static friction (stiction)} \end{cases} \quad (7)$$

In order to investigate the friction, we first remove the pendulum from the cart. The equation (3) reduces to:

$$F = M\ddot{x} + F_{fric} \quad (8)$$

Then, we apply a ramp voltage until the cart starts to move. At the instant the cart begins to move (i.e. $\dot{x} = \varepsilon \ll 1$), we evaluate the coulomb friction force using (5) and it is equal to b_0 . That is,

$$F_c \Big|_{\dot{x}=\varepsilon} = \frac{V_{in} K_t n}{Rr} \Big|_{\dot{x}=\varepsilon} = b_0 \quad (9)$$

Three additional sets of experiments are conducted on this setup where we apply higher F to overcome stiction while we are monitoring x and evaluating \dot{x}, \ddot{x} : **(i)** The cart pushes against a force transducer which is held fixed by a mechanical stop (thus $x = \dot{x} = \ddot{x} = 0$). This effort produces the torque constant (K_t), from (5). **(ii)** To determine the back-emf constant (K_e) and armature resistance (R), we use the following relation:

$$I_m = \frac{V_{in}}{R} - \frac{\dot{x} K_e n}{Rr} \quad (10)$$

where the motor current (I_m), the armature voltage (V_{in}) and the cart velocity (\dot{x}) are measured quantities. K_e and R are evaluated via the pursuant regression analysis. **(iii)** Several step function type V_{in} are deployed and the cart motion is monitored. This exercise produces the best estimate of viscous friction constant (b).

The frictional torque on the pendulum hub is modeled in a similar fashion to equation (6), as:

$$T_{fric} = c\dot{\theta} + T_c \quad (11)$$

where the coulomb friction torque, T_c , is defined as:

$$T_c = c_0 \operatorname{sgn}(\dot{\theta}), \quad \dot{\theta} \neq 0 \quad (12)$$

Note that due to frictionless bearings and lubrication at the hub there is no discernible stiction torque. To determine c and c_0 , we lock the cart on the rack (*i.e.* $x = \dot{x} = \ddot{x} = 0$) while the pendulum is in the downward position ($\theta = \pi$). Equation (2) when linearized around $\theta = \pi$ reduces to:

$$\frac{4m\ell^2 \ddot{\tilde{\theta}}}{3} + c\dot{\tilde{\theta}} + c_0 \operatorname{sgn}(\dot{\tilde{\theta}}) + mg\ell \tilde{\theta} = 0 \quad \text{where} \quad (13)$$

$$\tilde{\theta} = \theta - \pi$$

The equilibrium of $\theta = \pi$ ($\tilde{\theta} = 0$) is disrupted by an impulsive force on the pendulum and the pendulum's response is recorded. Using only the oscillation frequencies, damped natural frequency (ω_d) is numerically obtained. The natural frequency (ω_n) of the pendulum and the equivalent viscous friction constant (c) are calculated utilizing the following equations:

$$\omega_n = \sqrt{\frac{3g}{4\ell}}, \quad \omega_d = \omega_n \sqrt{1 - \zeta^2}, \quad \frac{8\omega_n \zeta m \ell^2}{3} = c \quad (14)$$

Then, the coulomb frictional torque (c_0) is determined applying an iterative numerical tool which compares the actual and simulated angular motions.

The Table 1 displays all the dynamic parameters obtained for the experimental setup used for the tests.

TABLE I
SYSTEM PARAMETER VALUES

M	0.911 kg	b_0	0.16 N
m	0.231 kg	n	3.7
l	0.32 m	R	2.87 Ω
K_t	0.00567 Nm/A	r	0.55 cm

K_e	0.00622 Vs	I	0.00788 kgm ²
b	8.4 Ns/m	g	9.8 m/s ²
c	0.0006 Nms/rad	c_0	0.0003 Nm

In order to validate these parameters, we apply an impulsive voltage to the DC motor, and record the uncontrolled pendulum response starting from the equilibrium of pendulum at downward position, $\theta = \pi$. We compare these recordings with the simulated behavior for the pendulum motion (Fig. 2). The correspondence between the experimental data and the simulation is very good.

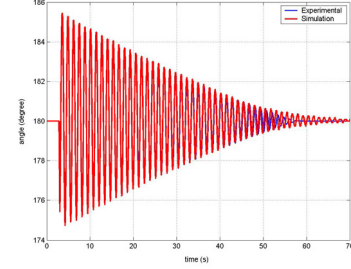


Fig. 2. Impulse response the angle of the pendulum obtained from the experiment (blue) and the simulation (red).

II. CONTROLLER DESIGN

Combining equations (3,4 and 5) and considering the desired trajectories, x_d and θ_d , one can obtain the state-space representation of the error dynamics as:

$$\dot{\mathbf{e}} = \mathbf{A}\mathbf{e} + \mathbf{B}V_{in} + \mathbf{E} \quad (15)$$

where $\mathbf{e} = \begin{bmatrix} x_d - x \\ \theta_d - \theta \\ \dot{x}_d - \dot{x} \\ \dot{\theta}_d - \dot{\theta} \end{bmatrix}$ state vector in error domain.

$$\mathbf{A} = \begin{bmatrix} 0 & 0 & 1 & 0 \\ 0 & 0 & 0 & 1 \\ 0 & \frac{-3mg}{(4M+m)} & \frac{-4(b+\beta)}{(4M+m)} & \frac{3c}{\ell(4M+m)} \\ 0 & \frac{3g(m+M)}{\ell(4M+m)} & \frac{3(b+\beta)}{\ell(4M+m)} & \frac{-3c(M+m)}{m\ell^2(4M+m)} \end{bmatrix}$$

$$\mathbf{B} = \begin{bmatrix} 0 \\ 0 \\ \frac{4\alpha}{(4M+m)} \\ \frac{-3\alpha}{\ell(4M+m)} \end{bmatrix}$$

$$\mathbf{E} = \begin{bmatrix} 0 \\ 0 \\ \frac{3c_0 \operatorname{sgn}(\dot{\theta})}{\ell(4M+m)} - \frac{4b_0 \operatorname{sgn}(\dot{x})}{(4M+m)} \\ \frac{-3c_0(M+m) \operatorname{sgn}(\dot{\theta})}{m\ell^2(4M+m)} + \frac{3b_0 \operatorname{sgn}(\dot{x})}{\ell(4M+m)} \end{bmatrix} \quad \text{is the}$$

disturbance (friction) term.

This is the SISO model (V_{in} vs. x or V_{in} vs. θ), that we wish to deploy for the design of a feedback control law using linear quadratic regulator (LQR) optimal control

method. This technique determines the feedback gain matrix that minimizes a linear quadratic cost function J .

$$J = \int_0^{\infty} (\mathbf{e}^T \mathbf{Q} \mathbf{e} + V_{in}^T R V_{in}) dt \quad (16)$$

where \mathbf{Q} is a positive-definite real matrix and $R \in \mathfrak{R}^+$. The \mathbf{Q} and R terms determine the relative importance of the error and the expenditure of the control energy, respectively. We make the following arbitrary selections for this study:

$$\mathbf{Q} = \begin{bmatrix} 4500 & 0 & 0 & 0 \\ 0 & 3000 & 0 & 0 \\ 0 & 0 & 30 & 0 \\ 0 & 0 & 0 & 30 \end{bmatrix}, R = 1 \quad (17)$$

Using these weighting values, the optimum state feedback gain vector is found from LQR as:

$$\mathbf{K} = [-67.08 \quad -162.16 \quad -57.87 \quad -31.96] \quad (18)$$

with which the full state feedback control law forms as $V_{in} = \mathbf{K} \mathbf{e}$. The practical implementation of any control law must also account for the actuator saturation possibility. Therefore, the desired trajectories x_d and θ_d must be selected within the limitations of the existing actuator. We perform a simulation study prior to the experiments and assure that this condition is satisfied.

III. TIME DELAY EFFECT IN THE FEEDBACK

The control gain in (18) is based on a non-delayed feedback setting. When the delays appear in the feedback loop, the trajectory tracking ability of the system is directly influenced. Since the controlled dynamics has to be stable in order to achieve a desirable tracking, we query the stability of the system with respect to the delays. In our system, we consider a delay, τ_1 , in the feedback line of x , \dot{x} and another delay, τ_2 , for θ , $\dot{\theta}$. We rewrite the error dynamics of the delayed feedback system from (15) excluding the disturbance term \mathbf{E} :

$$\dot{\mathbf{e}} = \mathbf{A} \mathbf{e} + \mathbf{B} \mathbf{K}_1 \mathbf{e}(t - \tau_1) + \mathbf{B} \mathbf{K}_2 \mathbf{e}(t - \tau_2) \quad (19)$$

where the control law is

$$V_{in} = \mathbf{K}_1 \mathbf{e}(t - \tau_1) + \mathbf{K}_2 \mathbf{e}(t - \tau_2).$$

Equation (19) represents a general class of linear-time invariant (LTI) multiple time delayed system (MTDS). The feedback gain \mathbf{K} is separated into two segments, \mathbf{K}_1 and \mathbf{K}_2 , as:

$$\mathbf{K}_1 = [-67.08 \quad 0 \quad -57.87 \quad 0] \\ \mathbf{K}_2 = [0 \quad -162.16 \quad 0 \quad -31.96]$$

components of which are selected from (18). The characteristic equation of the dynamics in equation (19) becomes:

$$CE(s, \tau_1, \tau_2) = \det \left[s \mathbf{I} - \mathbf{A} - \mathbf{B} \sum_{j=1}^2 \mathbf{K}_j e^{-\tau_j s} \right] = 0 \quad (20)$$

Considering the presence of multiple delays, we further broaden the aim of this study to manipulate the time delays and ensure the stability. Since we can not shorten the existing delays due to the causality principle, ‘manipulating’ means to add artificial delays to the inherent delays in the

system. This manipulation is in fact a ‘scheduling’ activity on the delays. For a successful delay scheduling, we need to determine all delay pairs which ensure the stability of the system. This complex problem is handled by a recent procedure, called the Cluster Treatment of Characteristic Roots (CTCR). Here, we will give only the key propositions of CTCR paradigm and refer the interested reader to [10, 13, 14].

Proposition 1 states that equation (20) can have an imaginary root at $s = \pm \omega_c i$ (where c denotes crossing) only along a bounded number of hypersurfaces $(\tau_1, \tau_2) \in \mathfrak{R}^{2+}$. These hypersurfaces (or simply ‘curves’ in 2-D space) are indeed offspring of a manageably small number of hypersurfaces which are called ‘kernel hypersurfaces’. And kernel hypersurfaces are defined as the locus of $\min\{\tau_1, \tau_2\}_{\omega_c} = \{\tau_{10}, \tau_{20}\}_{\omega_c}$, $\{\tau_1, \tau_2\} \in \mathfrak{R}^{2+}$ for all possible ω_c . The notation $\{\tau_1, \tau_2\}_{\omega_c}$ declares that $\{\tau_1, \tau_2\}$ pair causes a root of $\omega_c i$ for (20). Every point $\{\tau\}$ generated by (20) causes the same imaginary characteristic root $\omega_c i$. That is, $\{\tau\}_{\omega_c}$ holds. The loci obtained from the kernel using the following transformation point-by-point are called the ‘offspring’.

$$\{\tau\} = \left\{ \tau_{10} + \frac{2\pi}{\omega_c} j, \tau_{20} + \frac{2\pi}{\omega_c} k \right\}, j = 1, 2, \dots, k = 1, 2, \dots \quad (21)$$

The root tendencies of each purely imaginary characteristic root crossing, $\omega_c i$, with respect to one of the time delays is defined as:

$$S_{\tau_j}^s \Big|_{s=\omega_c i} = \frac{ds}{d\tau_j} \Big|_{s=\omega_c i} = \frac{\frac{\partial CE}{\partial \tau_j}}{\frac{\partial CE}{\partial s}} \Big|_{s=\omega_c i}, \quad i = \sqrt{-1}, \quad j = 1, 2 \quad (22)$$

The corresponding root tendency with respect to one of the delays is given as:

$$\text{Root Tendency} = RT \Big|_{s=\omega_c i} = \text{sgn} \left[\text{Re} \left(S_{\tau_j}^s \Big|_{s=\omega_c i} \right) \right] \quad (23)$$

Proposition 2 states that the root tendency at a crossing frequency, ω_c , caused by a delay pair $\{\tau_{10}, \tau_{20}\}$ on the kernel hypersurface is invariant when one of the delays is fixed. That means, the imaginary root always crosses either to unstable right half plane (for $RT = +1$) or to the stable left half plane (for $RT = -1$), when one of the delays is kept fixed, and the other one skipped from one offspring to the next, regardless of the actual time delays as long as they are derived from the same kernel $\{\tau_{10}, \tau_{20}\}$ point. These tendencies will give the complete stability switching regime for all the offspring curves.

Following the structured steps described in [13], we obtain the complete and exhaustive ‘stability map’ of the system within the $0 < \tau_1 < 180\text{ms}$ and $0 < \tau_2 < 170\text{ms}$ region (see Fig. 3). The shaded regions are stable operating points.

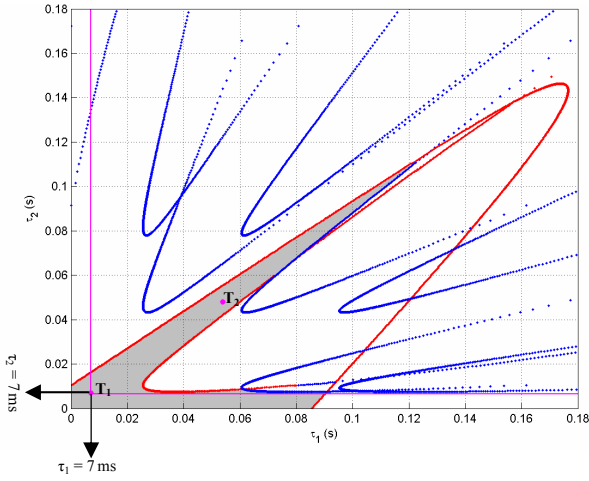


Fig. 3. The complete stability map of the multiple time-delayed cart-pendulum system in the domain of the delays.

IV. EXPERIMENTAL WORK

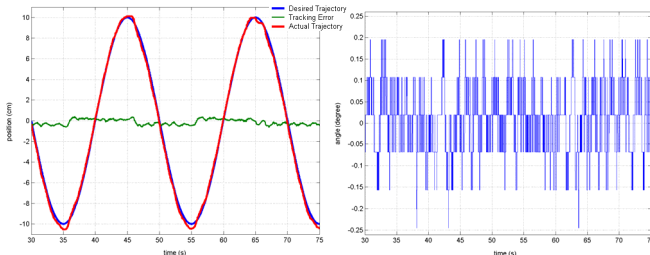
The stability features of the system as depicted in Fig. 3 are validated in this section. The digital control features are: sampling speed is 1 kHz, inherent delay within the system (from sensing to actuation) is 7 ms, that is, the control loop has a minimum 7 ms unavoidable delay. The resolution of the angular motion (θ) is 0.088° which is the capability obtained by a 4096 pulses/rev encoder. With another identical encoder, we obtain the cart position (x) with a resolution of 23 μm . A filtered differentiator whose bandwidth is much larger than the system bandwidth is utilized for the cart velocity (\dot{x}) and the pendulum angular velocity ($\dot{\theta}$) calculations. Note that the actuator is expected to remain within its linear range and without an occurrence of saturation for all experiments. We performed two sets of experiments on this system.

A. Trajectory Tracking Tests

The desired cart trajectory is taken as

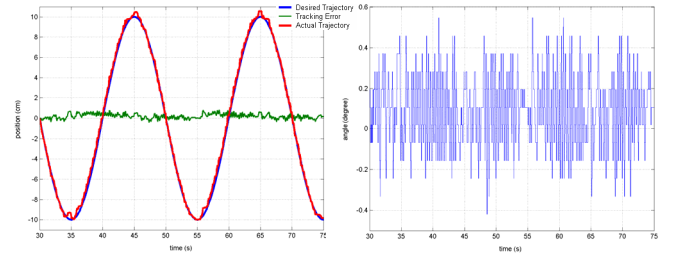
$$x_d(t) = 10 \sin(0.1\pi t) \text{ cm} \quad (24)$$

while performing a regulation on θ (that is, $\theta_d = 0$). The steady-state tracking performances are obtained for two stable test points T_1 ($\tau_1 = 7 \text{ ms}, \tau_2 = 7 \text{ ms}$) and T_2 ($\tau_1 = 54 \text{ ms}, \tau_2 = 48 \text{ ms}$) (see Fig. 3). The corresponding experimental results are shown in Fig. 4 for T_1 and in Fig. 5 for T_2 .



(a) The desired trajectory (blue), actual trajectory (red) and the tracking error (green) of the cart.
(b) Angle (θ) variation during the trajectory tracking.

Fig. 4. Experimental results for point T_1 ($\tau_1 = 7 \text{ ms}, \tau_2 = 7 \text{ ms}$).



(a) The desired trajectory (blue), actual trajectory (red) and the tracking error (green) of the cart.
(b) Angle (θ) variation during the trajectory tracking.

Fig. 5. Experimental results for point T_2 ($\tau_1 = 54 \text{ ms}, \tau_2 = 48 \text{ ms}$).

Fig. 4a displays a very good tracking ability of the cart motion. Notice that at the peak points of the actual position trajectory, there are some small fluctuations due to stick-slip motion between the rack and the driver pinion. The pinion is sliding in a jerky fashion because of the stiction force. Fig. 4b shows small angular errors within the bounds of ± 2 times the resolution of the optical sensor. Figs. 5a, b are displaying the similar comparative picture between the evaluated and measured quantities but for much larger delays. These two cases represent the stable tracking, while a selection of (τ_1, τ_2) in an unstable region of Fig. 3 causes instability (not shown here).

The conclusion one can reach, is that if the feedback lines have some unavoidable delays, we can purposely increase them to bring the operating point to within the stable (shaded) zone of Fig. 3. This is what we call the ‘delay scheduling’ strategy [9, 11].

B. Disturbance Rejection Tests

On this stability map, we also check the control performance variations. The dominant time constant γ_{dominant} of the system is directly related to the disturbance rejection speed:

$$\gamma_{\text{dominant}} = \frac{1}{|\text{Re}(s_{\text{dominant}})|} \quad (25)$$

where s_{dominant} is the rightmost characteristic root of the system. A numerical code [16] is used to find the rightmost characteristic root for a given point in (τ_1, τ_2) space. For point T_1 ($\tau_1 = 7 \text{ ms}, \tau_2 = 7 \text{ ms}$), the real part of the rightmost pole is found at -2.75 while for point T_2 ($\tau_1 = 54 \text{ ms}, \tau_2 = 48 \text{ ms}$), it is at -3 . This implies that for this delayed feedback structure; the settling time gets even better by increasing the delays from T_1 to T_2 . Otherwise said, we can reschedule the delays to enhance the control performance without changing the control law. This is probably the most impressive utilization of CTCR in practice.

The trajectory tracking operation using the delays at point T_2 , is tested next, from the disturbance rejection perspective. For these tests, we disrupt the controlled tracking operation in two different ways:

1st type of disturbance: An impulsive torque is applied on the DC motor while it is following the desired trajectory.

2nd type of disturbance: A small impulsive force is executed on the pendulum while the cart is following the

desired trajectory. In both cases, the settling times should be identical, since the rightmost poles remain unchanged.

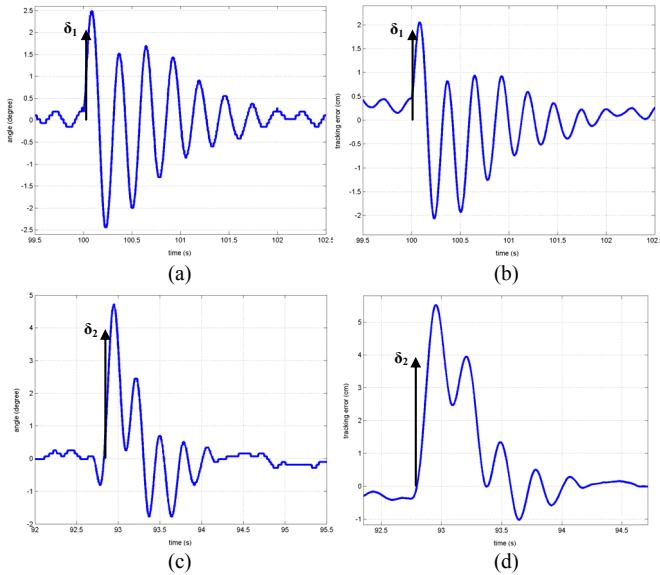


Fig. 6. For point T_2 ($\tau_1 = 54$ ms, $\tau_2 = 48$ ms)

Experimental response of (a) angle and (b) tracking error for the 1st type of disturbance (δ_1).

Experimental response of (c) angle and (d) tracking error for the 2nd type of disturbance (δ_2).

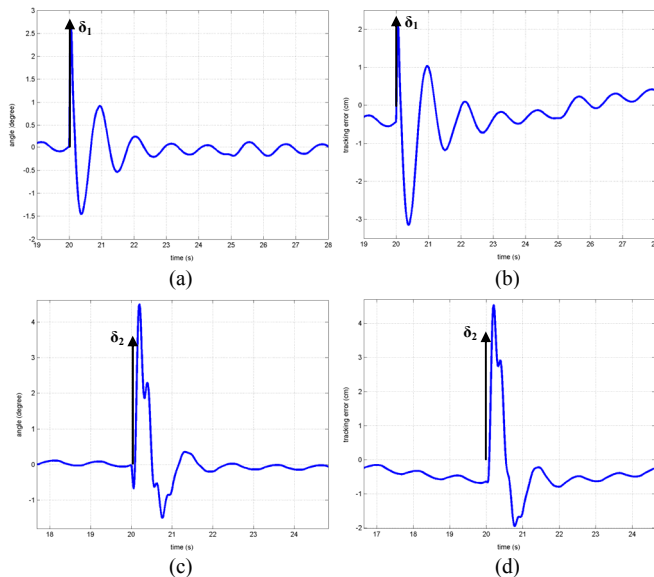


Fig. 7. For point T_2 ($\tau_1 = 54$ ms, $\tau_2 = 48$ ms)

Simulation response of (a) angle and (b) tracking error for the 1st type of disturbance (δ_1).

Simulation response of (c) angle and (d) tracking error for the 2nd type of disturbance (δ_2).

In Fig. 6, for ($\tau_1 = 54$ ms, $\tau_2 = 48$ ms) delay pair, the disturbance rejection responses in angle and position are shown for both type of disturbances. For the 1st and 2nd disturbance types, the simulation results are also obtained and shown in Fig. 7. The behaviors match very closely, which again demonstrate the reliability of the model used. Note that, the steady state oscillations in the simulation responses are due to trajectory tracking and nonlinear friction model.

V. CONCLUSION

Trajectory tracking of an underactuated LTI-MTDS is studied. Multiple time delays are considered in the feedback line. First, the cart-and-pendulum system has been modeled and the relevant componentwise identification tests are carried out. Second, a stability analysis for the controlled system is done utilizing a recent procedure called CTCR. We show that the delays can be increased for an improved control performance based on the stability map obtained with CTCR in the domain of delays. The confidence with this claim and the fidelity of the mathematical model utilized are also shown experimentally. It's observed that trajectory tracking can still be successful for some larger delays while improving the disturbance rejection capabilities of the system.

REFERENCES

- [1] Angeli, D.: 'Almost global stabilization of the inverted pendulum via continuous state feedback', *Automatica*, 2001, Volume 37, Issue 7, Pages 1103-1108.
- [2] Astrom, K.J., Furuta, K.: 'Swinging up a pendulum by energy control', *Automatica*, 2000, 36 287-295.
- [3] Atay, F.M.: 'Balancing the inverted pendulum using position feedback', *Applied Mathematics Letters*, 1999, 12, 51-56.
- [4] Brock, S.: 'Identification of the parameters in inverted pendulum model', 7th International Workshop on Advanced Motion Control; proceedings, 2002.
- [5] Casavola, A., Mosca, E., Papini, M.: 'Predictive teleoperation of constrained dynamic systems via internet-like systems', *IEEE Transactions on Control Systems Technology*, 2006, 14 (4), pp. 681-694.
- [6] Franklin, G.F., Powell, J.D., Naeni, A.E.: 'Feedback control of dynamic systems' (Prentice Hall, 2002, 3rd edn.).
- [7] Landry, M., Campbell, S.A., Morris, K., Aguilar, C.O.: 'Dynamics of inverted pendulum with delayed feedback control', *SIAM Journal of Applied Dynamical Systems*, 2005, Vol. 4, No.2, pp.333-351.
- [8] Olfati-Saber, R.: 'Fixed Point Controllers and Stabilization of the Cart-pole System and the Rotating Pendulum', *Proceedings of the IEEE Conference on Decision and Control* 2, 1999, p 1174-1181.
- [9] Olgac, N., Ergenc, A.F., Sipahi, R.: 'Delay scheduling': a new concept for stabilization in multiple delay systems', *Journal of Vibration and Control*, 2005, v 11, n 9, p 1159-72.
- [10] Olgac, N., Sipahi, R.: 'An exact method for the stability analysis of time-delayed LTI systems', *IEEE Transactions on Automatic Control*, 2002, 47(5), 793-797.
- [11] Olgac, N., Sipahi, R., Ergenc, A.F.: 'Delay scheduling', an unconventional use of time delay for trajectory tracking', *Mechatronics*, 2007, 17 (4-5), pp. 199-206.
- [12] Rao, S.S.: 'Mechanical Vibrations', (Addison-Wesley, 1995, 3rd edn.).
- [13] Sipahi, R., Olgac, N.: 'Complete stability robustness of third-order LTI multiple time-delay systems', *Automatica*, 2005, v 41, n 8, p 1413-22.
- [14] Sipahi, R., Olgac, N.: 'A unique methodology for the stability robustness of multiple time delay systems', *Systems & Control Letters*, 2006, (55) 819 – 825.
- [15] Spong, M.W.: 'Energy based control of a class of underactuated mechanical systems', *Proceedings of the 13th World Congress, International Federation of Automatic Control. Vol.F. Nonlinear Systems II*, 1997, 431-5.
- [16] Vyhldal, T. and Zitek, P.: 'Quasipolynomial mapping based rootfinder for analysis of time delay systems', *Proc IFAC Workshop on Time-Delay Systems, TDS'03*, 2003.
- [17] Zhao Jun, and Spong, M.W.: 'Hybrid control for global stabilization of the cart-pendulum system', *Automatica*, 2001, 37(12):1941-1951.